

MULTI-SCALE DEFECT DETECTION NETWORK FOR TIRE X-RAY IMAGES

Ren Wang^{1,2}, Qiang Guo^{1,2}, Caiming Zhang³

¹School of Computer Science and Technology,
Shandong University of Finance and Economics, Jinan, China

²Shandong Provincial Key Laboratory of Digital Media Technology, Jinan, China

³Software College, Shandong University, Jinan, China

ABSTRACT

Though automatic detection method has been tremendous improved, with the gradual penetration of deep learning. Defect detection in many industrial processes is one of the remaining challenging tasks due to the diversity of its products. In this work, we focus on detection tasks in tire industry and develop a *Multi-scale Defect Detection Network (MDDN)*, which contains two parallel sub-networks to capture multi-scale defect features. Specifically, high-abstracted semantic features containing defect shapes and locations are mined via a *Semantic-aware sub-network*, simplified by an off-the-shelf fully convolutional network. Furthermore, to complement the details filtered by the deep network, a novel *Texture-aware Sub-network* is used to exploit the small size of the cover edge features and small defects as much as possible. Finally, the pixel-wised detection results are obtained by fusing features with semantic and texture information. Extensive experiments demonstrate that *MDDN* can produce comparable results and achieve significantly performance improvement in small defects detection.

Index Terms— Defect detection, Fully convolutional network, Semantic segmentation, Multi-scale context

1. INTRODUCTION

Automatic defect detection, used to improve quality and accelerate production, has become an indispensable part in industrial processes, such as fabrics[1, 2, 3], steel[4], semiconductors[5], and solar wafers[6]. Especially in tire manufacturing, numerous detection algorithms have been proposed[7, 8, 9, 10, 11] and aroused extensive attention over the past two decades. In most real-world applications, tire defect detection is first carried out by deriving the defective region from tire X-ray images, which contains various types of defects caused by unclean raw materials and undesired manufacturing facilities[12]. Then, the defective product is hierarchical processed according to the location and size of defects. Due to unique properties of the tire image, for instance complexity and low-quality, illustrated in previous study[13, 14], most inspection processes are performed by

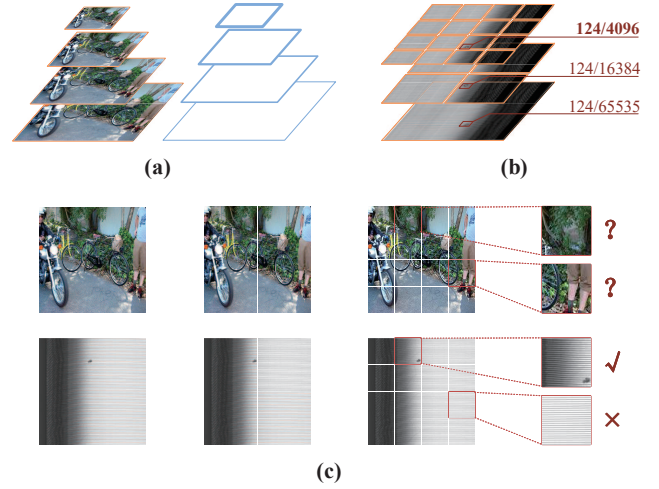


Fig. 1. Detection results of several benchmark architecture. (a) shows input tire images with different defects. From top to bottom, the first four are tire sidewall images, which involve following defect types: impurity, overlap, slack, bubble. The last two are tire tread images, which involve overlaps.

human observers, which increases the risk and reduces the efficiency. Therefore, tire defect detection remains one of the most challenging inspection tasks.

At present, existing computer vision based detection methods are mostly devoted to distinguish difference between defective regions and background (defective-free regions). Hence a key issue for such methods is feature extraction. Guo *et al.*[11] exploited a local kernel regression descriptor to derive feature vectors. By comparing the dissimilarity of the corresponding feature between one pixel and its neighbors, anomaly pixels can be located and segmented, even in the tread image. Nevertheless, this method is not suitable for real-time detection tasks because of the high computational complexity. A component decomposition based method was proposed in[12], which separated the background from the image by means of two designed filters.

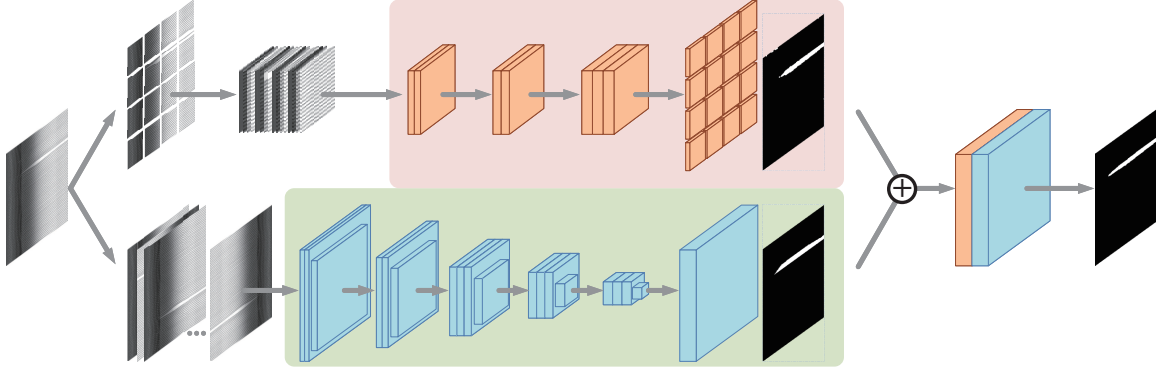


Fig. 2. Detection results of several benchmark architecture. (a) shows input tire images with different defects. From top to bottom, the first four are tire sidewall images, which involve following defect types: impurity, overlap, slack, bubble. The last two are tire tread images, which involve overlaps.

Then through an adaptive thresholding processing, defects were derived from the residual image. Besides, Independent component analysis(ICA) was also used for defect detection tasks[8, 9]. A major disadvantage of these fundamental methods is the limitation of the information contained in low-level clues and domain features. To address the limitation, Zhang *et al.*[7] and Zhang *et al.*[13] introduced radon transform and multi-scale transform, for instance curvelet and wavelet transform, in detection tasks respectively. Furthermore, optimized edge detection and total variation algorithm are used to achieve more accurate results[15]. Zhao *et al.*[16] proposed a multiple kernel learning method, which combined various transform kernels to get more differentiated information. However, the representation capability of fixed kernels is not comprehensive enough. In addition, transform process is computationally expensive. Recently, Cui *et al.*[17] attempted to classify tire defects by means of convolutional neural networks(CNN), which has outstanding performance in the recognition and segmentation tasks of natural images. With the excellent feature extraction capability of deep network, Wang *et al.*[14] further implemented the detection and segmentation in tire images by a fully convolutional network(FCN)[18]. However, FCN is not sensitive to small defects and edge details, which is similar to that in dealing with natural image tasks.

To overcome the shortcomings of insensitivity to small defects and detailed textures, many methods have been proposed in benchmark datasets. Most of them are based on multi-scale strategies and can be roughly classified into image pyramids and in-network feature hierarchies. Image pyramids illustrated in Figure 1a[] were extensively used in the era of hand-crafted features[19, 20]. Even if the crafted features have largely been replaced by self-learning features, multi-scale testings on the image pyramid are still used to verify the adaptability and robustness. Nevertheless, image pyramid based methods is impractical for real applications due to the considerable increase in inference time. In-network fea-

ture hierarchies are formed by the forward propagation within deep convolutional networks(ConvNets). Due to a series of sub-sampling layers, in-network hierarchies produce feature maps of different spatial resolutions, with an multi-scale and pyramid shape[]. By fusing these multi-scale feature maps, the texture feature in shallow layers and the semantic information contained in deep layers can be perceived. The Single Shot Detector (SSD) [] is one of the first attempts at combining predictions from these features maps to detect objects of various sizes. Generally, shallow features are used to predict small objects, and deep features with large receptive fields are used detect large objects. However, the lack of semantic information is harmful to the detection of small targets in shallow layers. Another fusing way can effectively address this problem by concatenating multi-scale features and detecting on top of the expanded feature maps, as shown by the red line in Figure 1b[]. For example, FCN-8s and FNC-16s defined a skip architecture to produce more accurate segmentation. Similar top-down skip architectures are popular in recent research[]. There exists a basic problem that it is still not enough to mine the detail texture in these structures[]. Moreover, small targets will become smaller or even disappear as the increases of sub-sampling layers, even if they can be captured in shallow layers.

Inspired by MTGAN, we construct a end-to-end network named Multi-scale Defect Detection Network (MDDN) consisting of a semantic-aware sub-network and a texture-aware sub-network. Based on tire X-ray images, a image patch s-trategy is adopted in the texture-aware sub-network. Unlike natural image patches, defects (objects) are still significant and discernible in the tire image patches, as shown in Figure 1(c). On the one hand, The proportion of the area of defective regions in images increases, which is advantageous for better capturing of detailed information. As shown in Figure 1(b), for a 256*256 tire image, the proportion of defects is increased from *** to ***. On the other hand, image patches as input data can be used without reducing the number of

parameters in the case of reducing the pooling layer. On the other hand, sub-sampling layers can be discarded to retain more shallow features without increasing the parameters.

2. MULTI-SCALE DEFECT DETECTION NETWORK

All printed material, including text, illustrations, and charts, must be kept within a print area of 7 inches (178 mm) wide by 9 inches (229 mm) high. Do not write or print anything outside the print area. The top margin must be 1 inch (25 mm), except for the title page, and the left margin must be 0.75 inch (19 mm). All *text* must be in a two-column format. Columns are to be 3.39 inches (86 mm) wide, with a 0.24 inch (6 mm) space between them. Text must be fully justified.

All printed material, including text, illustrations, and charts, must be kept within a print area of 7 inches (178 mm) wide by 9 inches (229 mm) high. Do not write or print anything outside the print area. The top margin must be 1 inch (25 mm), except for the title page, and the left margin must be 0.75 inch (19 mm). All *text* must be in a two-column format. Columns are to be 3.39 inches (86 mm) wide, with a 0.24 inch (6 mm) space between them. Text must be fully justified.

All printed material, including text, illustrations, and charts, must be kept within a print area of 7 inches (178 mm) wide by 9 inches (229 mm) high. Do not write or print anything outside the print area. The top margin must be 1 inch (25 mm), except for the title page, and the left margin must be 0.75 inch (19 mm). All *text* must be in a two-column format. Columns are to be 3.39 inches (86 mm) wide, with a 0.24 inch (6 mm) space between them. Text must be fully justified.

All printed material, including text, illustrations, and charts, must be kept within a print area of 7 inches (178 mm) wide by 9 inches (229 mm) high. Do not write or print anything outside the print area. The top margin must be 1 inch (25 mm), except for the title page, and the left margin must be 0.75 inch (19 mm). All *text* must be in a two-column format. Columns are to be 3.39 inches (86 mm) wide, with a 0.24 inch (6 mm) space between them. Text must be fully justified.

All printed material, including text, illustrations, and charts, must be kept within a print area of 7 inches (178 mm) wide by 9 inches (229 mm) high. Do not write or print anything outside the print area. The top margin must be 1 inch (25 mm), except for the title page, and the left margin must be 0.75 inch (19 mm). All *text* must be in a two-column format. Columns are to be 3.39 inches (86 mm) wide, with a 0.24 inch (6 mm) space between them. Text must be fully justified.

All printed material, including text, illustrations, and charts, must be kept within a print area of 7 inches (178 mm) wide by 9 inches (229 mm) high. Do not write or print anything outside the print area. The top margin must be 1

inch (25 mm), except for the title page, and the left margin must be 0.75 inch (19 mm). All *text* must be in a two-column format. Columns are to be 3.39 inches (86 mm) wide, with a 0.24 inch (6 mm) space between them. Text must be fully justified.

All printed material, including text, illustrations, and charts, must be kept within a print area of 7 inches (178 mm) wide by 9 inches (229 mm) high. Do not write or print anything outside the print area. The top margin must be 1 inch (25 mm), except for the title page, and the left margin must be 0.75 inch (19 mm). All *text* must be in a two-column format. Columns are to be 3.39 inches (86 mm) wide, with a 0.24 inch (6 mm) space between them. Text must be fully justified.

3. EXPERIMENTS

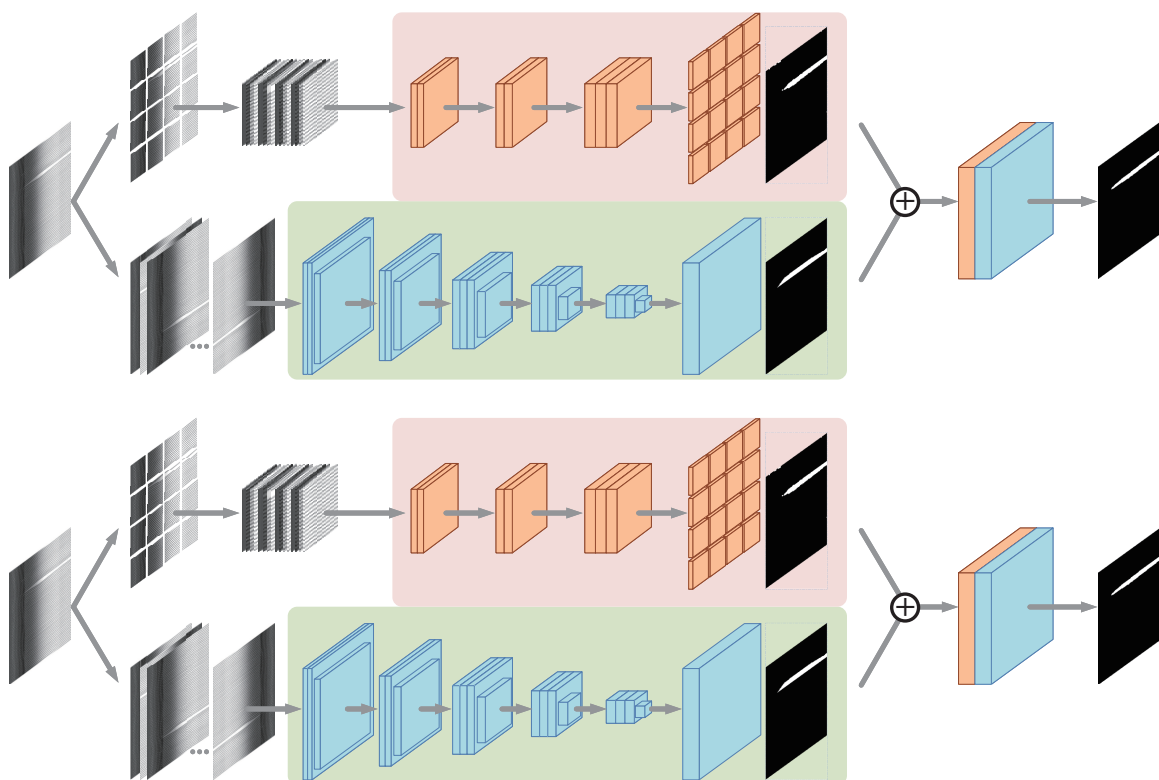
The paper title (on the first page) should begin 1.38 inches (35 mm) from the top edge of the page, centered, completely capitalized, and in Times 14-point, boldface type. The authors' name(s) and affiliation(s) appear below the title in capital and lower case letters. Papers with multiple authors and affiliations may require two or more lines for this information. Please note that papers should not be submitted blind; include the authors' names on the PDF. The paper title (on the first page) should begin 1.38 inches (35 mm) from the top edge of the page, centered, completely capitalized, and in Times 14-point, boldface type. The authors' name(s) and affiliation(s) appear below the title in capital and lower case letters. Papers with multiple authors and affiliations may require two or more lines for this information. Please note that papers should not be submitted blind; include the authors' names on the PDF.

The paper title (on the first page) should begin 1.38 inches (35 mm) from the top edge of the page, centered, completely capitalized, and in Times 14-point, boldface type. The authors' name(s) and affiliation(s) appear below the title in capital and lower case letters. Papers with multiple authors and affiliations may require two or more lines for this information. Please note that papers should not be submitted blind; include the authors' names on the PDF.

3.0.1. Sub-subheadings

Since there are many ways, often incompatible, of including images (e.g., with experimental results) in a LaTeX document, below is an example of how to do this [20].

List and number all bibliographical references at the end of the paper. The references can be numbered in alphabetic order or in order of appearance in the document. When referring to them in the text, type the corresponding reference number in square brackets as shown at the end of this sentence [20][21, 5, 8, 9, 17, 20, 4, 12, 11, 1, 3, 22, 23, 18, 19, 2, 6, 14, 24, 15, 13, 25, 7, 10, 16, 26, 27]. An additional final page (the



fifth page, in most cases) is allowed, but must contain only references to the prior literature.

additional final page (the fifth page, in most cases) is allowed, but must contain only references to the prior literature.

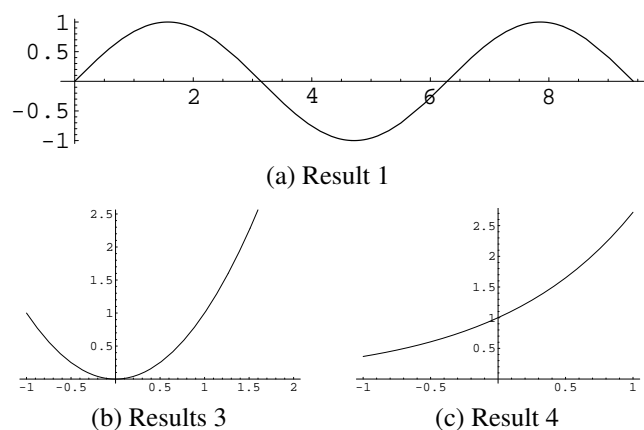


Fig. 3. Example of placing a figure with experimental results.

4. CONCLUSION

To achieve the best rendering both in printed proceedings and electronic proceedings, we strongly encourage you to use Times-Roman font. In addition, this will give the proceedings a more uniform look. Use a font that is no smaller than nine point type throughout the paper, including figure captions.

In nine point type font, capital letters are 2 mm high. **If you use the smallest point size, there should be no more than 3.2 lines/cm (8 lines/inch) vertically.** This is a minimum spacing; 2.75 lines/cm (7 lines/inch) will make the paper much more readable. Larger type sizes require correspondingly larger vertical spacing. Please do not double-space your paper. TrueType or Postscript Type 1 fonts are preferred.

The first paragraph in each section should not be indented, but all the following paragraphs within the section should be indented as these paragraphs demonstrate.

3.0.2. Sub-subheadings

List and number all bibliographical references at the end of the paper. The references can be numbered in alphabetic order or in order of appearance in the document. When referring to them in the text, type the corresponding reference number in square brackets as shown at the end of this sentence [20]. An

5. REFERENCES

- [1] A. Kumar, "Computer-vision-based fabric defect detection: A survey," *IEEE Trans. on Industrial Electronics*, vol. 55, no. 1, pp. 348–363, 2008.
- [2] H. Y. Ngan, G. K. Pang, and N. H. Yung, "Automated fabric defect detection: A review," *Image and Vision Computing*, vol. 29, no. 7, pp. 442–458, 2011.
- [3] Y. Li, W. Zhao, and J. Pan, "Deformable patterned fabric defect detection with fisher criterion-based deep learning," *IEEE Trans. on Automation Science and Engineering*, vol. 14, no. 2, pp. 1256–1264, 2016.
- [4] S. Ghorai, A. Mukherjee, M. Gangadaran, and P. K. Dutta, "Automatic defect detection on hot-rolled flat steel products," *IEEE Trans. on Instrumentation and Measurement*, vol. 62, no. 3, pp. 612–621, 2012.
- [5] X. Bai, Y. Fang, W. Lin, L. Wang, and B. F. Ju, "Saliency-based defect detection in industrial images by using phase spectrum," *IEEE Trans. on Industrial Informatics*, vol. 10, no. 4, pp. 2135–2145, 2014.
- [6] D. M. Tsai, S. C. Wu, and W. Y. Chiu, "Defect detection in solar modules using ica basis images," *IEEE Trans. on Industrial Informatics*, vol. 9, no. 1, pp. 122–131, 2012.
- [7] C. Zhang, X. Li, Q. Guo, X. Yu, and C. Zhang, "Texture-invariant detection method for tire crack," *Journal of Computer-Aided Design & Computer Graphics*, vol. 25, no. 6, pp. 809–816, 2013.
- [8] X. Cui, Y. Liu, and C. Wang, "Defect automatic detection for tire x-ray images using inverse transformation of principal component residual," in *AIPR. IEEE*, 2016, pp. 1–8.
- [9] X. H. Cui, Y. Liu, C. X. Wang, and H. Li, "A novel method for feature extraction and automatic recognition of tire defects using independent component analysis," *DEStech Transactions on Materials Science and Engineering*, no. icimm, 2016.
- [10] Y. Zhang, X. Cui, Y. Liu, and B. Yu, "Tire defect-classification using convolution architecture for fast feature embedding," *International Journal of Computational Intelligence Systems*, vol. 11, no. 1, pp. 1056–1066, 2018.
- [11] Q. Guo, C. Zhang, H. Liu, and X. Zhang, "Defect detection in tire x-ray images using weighted texture dissimilarity," *Journal of Sensors*, vol. 2016, 2016.
- [12] Q. Guo and Z. W. Wei, "Tire defect detection using image component decomposition," *Research Journal of Applied Sciences, Engineering and Technology*, vol. 4, no. 1, pp. 41–44, 2012.
- [13] Y. Zhang, T. Li, and Q. Li, "Defect detection for tire laser shearography image using curvelet transform based edge detector," *Optics & Laser Technology*, vol. 47, pp. 64–71, 2013.
- [14] R. Wang, Q. Guo, S. Lu, and C. Zhang, "Tire defect detection using fully convolutional network," *IEEE Access*, vol. 7, pp. 43502–43510, 2019.
- [15] Z. Yan, L. Tao, and L. Qing-Ling, "Detection of foreign bodies and bubble defects in tire radiography images based on total variation and edge detection," *Chinese Physics Letters*, vol. 30, no. 8, pp. 084205, 2013.
- [16] S. Zhao, Z. Chen, B. Li, and B. Zhang, "Tire x-ray image impurity detection based on multiple kernel learning," in *Pacific Rim Conference on Multimedia*. Springer, 2017, pp. 346–355.
- [17] X. Cui, Y. Liu, Y. Zhang, and C. Wang, "Tire defect-classification with multi-contrast convolutional neural networks," *International Journal of Pattern Recognition and Artificial Intelligence*, vol. 32, no. 04, pp. 1850011, 2018.
- [18] J. Long, E. Shelhamer, and T. Darrell, "Fully convolutional networks for semantic segmentation," in *Proceedings of the IEEE conference on computer vision and pattern recognition*, 2015, pp. 3431–3440.
- [19] D. G. Lowe, "Distinctive image features from scale-invariant keypoints," *IJCV*, vol. 60, pp. 91–110, 2004.
- [20] N. Dalal and B. Triggs, "Histograms of oriented gradients for human detection," in *CVPR*, 2005.
- [21] Y. Bai, Y. Zhang, M. Ding, and B. Ghanem, "Sodmtgan: Small object detection via multi-task generative adversarial network," in *ECCV*, 2018, pp. 206–221.
- [22] T. Y. Lin, P. Dollr, R. Girshick, K. He, B. Hariharan, and S. Belongie, "Feature pyramid networks for object detection," in *CVPR*, 2017, pp. 2117–2125.
- [23] W. Liu, D. Anguelov, D. Erhan, C. Szegedy, S. Reed, C. Y. Fu, and A. C. Berg, "Ssd: Single shot multibox detector," in *ECCV*. Springer, 2016, pp. 21–37.
- [24] C.D. Jones, A.B. Smith, and E.F. Roberts, "A dictionary-based method for tire defect detection," in *ICIA. IEEE*, 2014, pp. 519–523.
- [25] Y. Zhang, D. Lefebvre, and Q. Li, "Automatic detection of defects in tire radiographic images," *IEEE Trans. on Automation Science and Engineering*, vol. 14, no. 3, pp. 1378–1386, 2015.

- [26] P. Zhou, B. Ni, C. Geng, J. Hu, and Y. Xu, “Scale-transferrable object detection,” in *CVPR*, 2018, pp. 528–537.
- [27] L. C. Chen, Y. Yang, J. Wang, W. Xu, and A. L. Yuille, “Attention to scale: Scale-aware semantic image segmentation,” in *CVPR*, 2016, pp. 3640–3649.